

Arc Characteristics and Weld Bead Microstructure of Ti-6Al-4V Titanium Alloy in Ultra-high Frequency Pulse Gas Tungsten Arc Welding (UHFP-GTAW) Process

Wei LI¹, Gaochong LV¹, Qiang WANG², Songtao HUANG^{1*}

¹ Department of Electrical Engineering, Beijing Institute of Petrochemical Technology, No. 19 Qingyuan North Road, Huangcun Town, Daxing District, Beijing 102617, China

² China Aerospace Science and Industry Group Second Research Institute, Beijing 100854, China

crossref <http://dx.doi.org/10.5755/j01.ms.26.4.22329>

Received 19 December 2018; accepted 15 March 2019

To resolve the problem of grain coarsening occurring in the fusion zone and the heat-affected zone during conventional gas tungsten arc welding (C-GTAW) welded titanium alloy, which severely restricts the improvement of weld mechanical properties, welding experiments on Ti-6Al-4V titanium alloy by adopting ultra-high frequency pulse gas tungsten arc welding (UHFP-GTAW) technique were carried out to study arc characteristics and weld bead microstructure. Combined with image processing technique, arc shapes during welding process were observed by high-speed camera. Meanwhile the average arc pressure under various welding parameters were obtained by adopting pressure measuring equipment with high-precision. In addition, the metallographic samples of the weld cross section were prepared for observing weld bead geometry and microstructure of the fusion zone. The experimental results show that, compared with C-GTAW, UHFP-GTAW process provides larger arc energy density and higher proportion of arc core region to the whole arc area. Moreover, UHFP-GTAW process has the obviously effect on grain refinement, which can decrease the grain size of the fusion zone. The results also revealed that a significant increase of arc pressure while increasing pulse frequency of UHFP-GTAW, which could improve the depth-to-width ratio of weld beads.

Keywords: Ti-6Al-4V, ultra-high frequency pulse GTAW, arc behavior, grain refinement, basket-weave structure.

1. INTRODUCTION

Because of excellent comprehensive properties of high specific strength, well corrosion resistance and small density, titanium alloys have been widely used as important metal structural materials in various fields such as aerospace, transportation and medical treatment [1–5]. Gas tungsten arc welding (GTAW) process is a preferred method for welding of titanium alloys due to its expedient operability and low cost [6]. However, the problem of grain coarsening occurring in the fusion zone and the heat-affected zone severely restrict the improvement of weld mechanical properties during the GTAW process welded titanium alloy [7]. For obtaining grain refinement in weld fusion zones and improving the mechanical properties, pulsed current had been applied in GTAW process during past several decades [8–10]. It has been confirmed that introducing pulse current into the welding arc would exert remarkable influence on arc pressure, geometry of molten pool and the distribution of temperature field. Recently research results have also shown that, compared with conventional gas tungsten-arc welding (C-GTAW) process, pulsed gas tungsten-arc welding (P-GTAW) process has remarkable effect of refining grain size due to its lower heat input requirements and other advantages [8, 11]. There were also some results confirming that pulsed current frequency had a significant impact on the refinement of weld grain, and higher pulse frequency could get better effect on grain refinement [12–14].

In order to take the advantage of high-frequency pulse current as efficiently as possible, ultra-high frequency pulse GTAW (UHFP-GTAW) technique in which pulsed current frequency is up to 80 kHz has been developed to achieve better welding performance [15]. Previous research has proved that larger electromagnetic force help to increase weld penetration and higher central temperature of the molten pool in the weld bead can be obtained from UHFP-GTAW process [16]. In addition, with the implementation of related experiments on several metals including stainless steel, aluminum alloy and titanium alloy, ultra-high frequency pulsed current modulation of welding arc was proved to be effective on the crystallization process of the metal, and it is gradually confirmed that pulsed current with a frequency exceeding 20kHz have special effects on some aspects such as compressing arc shape, increasing weld penetration, refining grains and so on [17].

Arc behavior would exert directly impact on weld geometry and microstructure of weld seams, and then affect mechanical properties of weld bead. Considering that Ti-6Al-4V is the most commonly used titanium alloy, and in UHFP-GTAW process its weld quality is closely related to grain refinement degree, experimental research on arc behaviors and weld microstructures of Ti-6Al-4V titanium alloy by adopting UHFP-GTAW process were conducted to verify the validity of UHFP-GTAW process on grain refining.

* Corresponding author. Tel. : +86-10-81292758; fax: +86-10-81292758.
E-mail address: liweijpu@sohu.com (S.T. Huang)

2. METHODS

2.1. UHFP-GTAW technique

Based on parallel-connected circuit topology as shown in Fig. 1, the welding power source can achieve ultra-high frequency pulsed current output with frequency up to 80 kHz. Base current inverter and pulse current inverter can all produce corresponding constant current outputs named I_b and I_{pp} respectively, and I_{pp} is equivalent to the difference value between peak current I_p and base current I_b . The output effect of ultra-high frequency pulsed current depends on the fast alternation actions of two IGBTs (Insulated Gate Bipolar Transistor) named TP1 and TP2 at a certain frequency. The working principle is as follows: when TP1 turns on and TP2 off, the power source only provides base current I_b output; while TP1 turns off and TP2 on, the power source produces peak current I_p output. In particular, it should be noted that change rate of pulsed current rising and falling edges can reach 50 A/ μ s by taking appropriate protection and absorption measures. Actual welding current waveform is shown in Fig. 2.

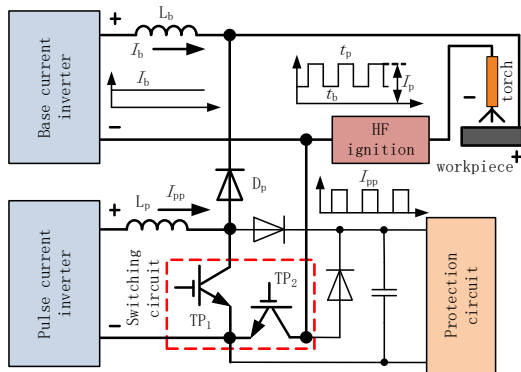


Fig. 1. Circuit topology of UHFP-GTAW power source

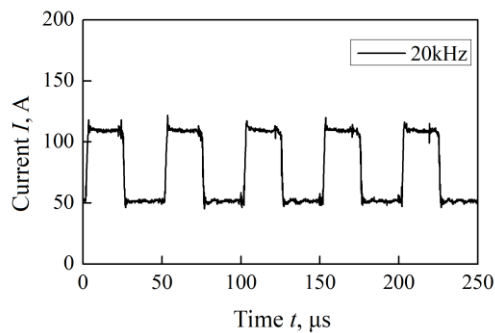


Fig. 2. Actual welding current waveform at frequency of 20 kHz

2.2. Arc profile capture

As shown in Fig. 3, a high-speed camera system is applied to capture arc profile, in which optical filters are employed to weaken the intensity of arc lights and protect camera lens. For ensuring arc stability and keeping focal length fixed during the welding process, workpiece moves in direction Y while welding torch and camera must be kept stationary. Arc profile captured by above means can be transferred to computer through communication cable.

The base metal used in this investigation is a high strength titanium alloy of Ti-6Al-4V and the chemical composition (wt.%) of the base metal is presented in

Table 1. Sheets of Ti-6Al-4V titanium alloy were cut into required sizes (100 mm \times 50 mm \times 5 mm).

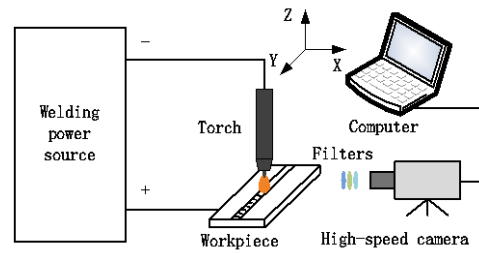


Fig. 3. Sketch of arc profile capture system

Table 1. Chemical composition (wt.%) of Ti-6Al-4V

Al	V	N	C	H	O	Fe	Ti
5.82	3.99	0.023	0.083	0.0007	0.063	<0.05	Balace

Before welding all the workpieces were sanded firstly, and then cleaned by alcohol. The shielding gas was argon with the purity of 99.99 % and the electrode with diameter of 2.4 mm is made up of 2 % cerium and 98 % tungsten. The distance between electrode and workpiece is 4 mm which was the arc length during welding. Welding current parameters are illustrated in Table 2, in which f , I_b , I_p , I_m respectively represents pulse frequency, base current, peak current and mean current. Meanwhile other parameters are kept fixed as follows: gas flow rate is 12 L/min, welding speed is 60 mm/min and duty cycle of pulse current is 50 %.

Table 2. Welding parameters

No.	f , kHz	I_b , A	I_p , A	I_m , A
1	—	60	—	60
2	20	40	80	60
3	40	40	80	60
4	—	80	—	80
5	20	50	110	80
6	40	50	110	80

2.3. Image processing

The bell-shaped photos captured were processed according to the procedures illustrated in Fig. 4 to obtain distinct boundaries. Original photo was initially converted into gray-scale map, and then areas outside arc column were removed from gray-scale map. The gray-scale map which only retains the arc column area was subsequently re-colored by using surface plot tool and contrast enhancement tool of the software called Image-Pro Plus. Post-processed arc column area was divided into three regions, where the red part is identified as arc core region I with the highest temperature, and the others as outer region II. The arc of core region I possessed the most concentrated plasma and the largest current density. The region I's area (S_I) and the region II's area (S_{II}), as well as projection diameter (D_I) of core region I were calculated through the software mentioned above.

2.4. Arc force measurement

As shown in Fig. 5 arc force measurement device is composed of a supporting mechanism with favorable rigidity and a precision electronic balance with accuracy of 0.01 g.

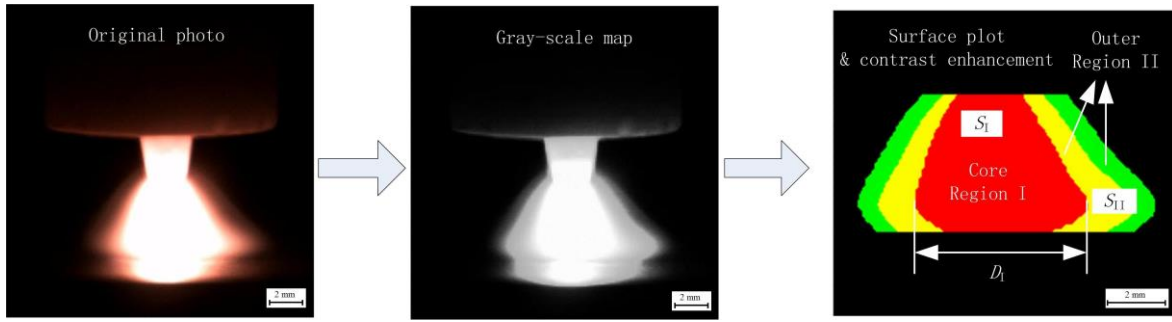


Fig. 4. Image processing steps

Workpiece is loaded on the top surface of insulated board to ensure electrical isolation with electronic balance. The pallet center of electronic balance should be kept consistent with that of insulated board, where arc force was measured and recorded for at least three times at each set of parameters shown in the Table 3. The validity of measurement results was ensured by means of taking average values from multiple measurements.

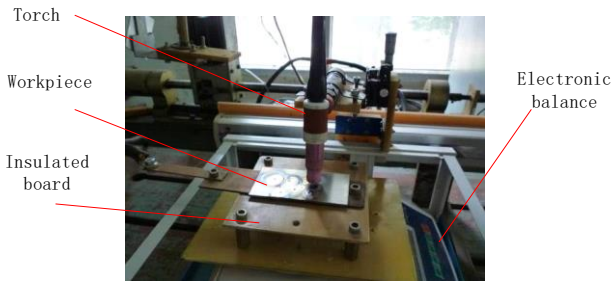


Fig. 5. Arc force measurement device

Table 3. Welding current parameters for arc force measuring

No.	f , kHz	Δ , %	I_b , A	I_p , A	I_m , A
1	—	—	60	—	60
2	5	50	40	80	60
3	10	50	40	80	60
4	20	50	40	80	60
5	40	50	40	80	60

3. RESULTS AND DISCUSSION

3.1. Arc profile

Photographs obtained during welding process corresponding to the various set of parameters listed in Table 2 were shown in Fig. 6. Table 4 shows the experimental results reflecting arc shape, among which the area ratio (R_I) of region I to the whole region which manifests the variation of arc profile was obtained directly by calculation, and the others were achieved according to the method of image processing introduced in Section 2. 3.

As shown in the first three rows of Table 4, under the condition of average current I_m of 60 A, the core area accounts for 38.9 % of the whole arc column area by C-GTAW process, and whereas in UHFP-GTAW mode, the proportion increases to 39.8 % and 40.6 % respectively with the pulse frequency of 20 kHz and 40 kHz. When average current enhanced to 80 A, the same trend also can be observed. Fig. 7 illustrates the variation trend of R_I more intuitively.

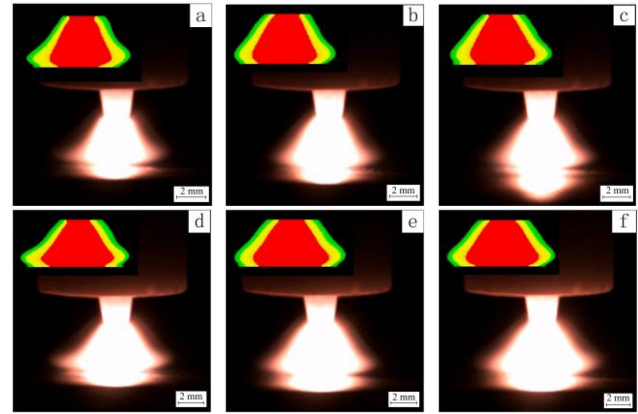


Fig. 6. Arc profiles captured by high-speed camera. Photographs a–f are in correspondence with 1–6 in Table 2.

Table 4. Calculated size of region I and II

No.	S_I , mm ²	S_{II} , mm ²	R_I , %	D_I , mm
1	15.12	23.72	38.9	4.24
2	15.94	24.11	39.8	4.69
3	16.63	24.32	40.6	4.76
4	19.13	24.21	44.2	5.71
5	20.99	25.93	44.7	5.97
6	20.83	25.15	45.3	6.14

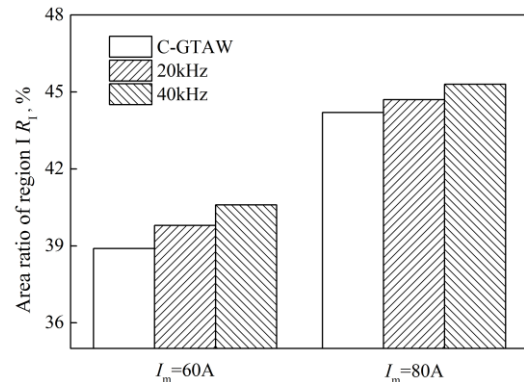


Fig. 7. Variation trends of the area ratio of core region I

3.2. Arc force and arc pressure

With average current of 60 A the influence of pulse frequency on the arc force is illustrated in Fig. 8, it needs to be pointed out that at each frequency arc force were measured three times and the value denoted by star symbol represents average arc force calculated from three tested results. As shown in Fig. 8, obvious increase over 30 percent was achieved by UHFP-GTAW process compared

with that of C-GTAW ($f=0$) process, and the higher the pulse frequency, the greater the average arc force. The maximum arc force occurs at frequency of 40 kHz, and increases by about 80.6 % compared with that of C-GTAW.

Arc pressure can be calculated by Eq. 1:

$$P_{\text{arc}} = F_{\text{arc}} / (\pi r^2), \quad (1)$$

where P_{arc} is arc pressure, $F_{\text{arc}} = mg$ represents arc force ($g = 10 \text{ N/kg}$), and r is radius of arc column melting metal of workpieces, i. e., half width of molten pool respectively. Considering that the width of the molten pool equals approximately to D_1 , so r can be replaced by $0.5 D_1$. Hence, Eq. 1 can also be expressed as Eq. 2.

$$P_{\text{arc}} = \frac{mg}{\pi(0.5D_1)^2}. \quad (2)$$

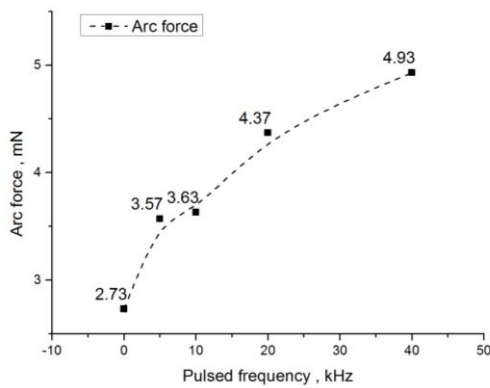


Fig. 8. Arc force at different pulsed current frequencies

As measured in Section 2.1, when average welding current adopted was 60 A, corresponding to 0 kHz, 20 kHz and 40 kHz, projection diameter D_1 is 4.24 mm, 4.69 mm and 4.76 mm respectively. According to Eq. 2 arc pressure was calculated to be 193.4 Pa, 253.1 Pa and 277.2 Pa at C-GTAW, 20 kHz and 40 kHz. It was obvious that arc pressure significantly increases when the pulsed current frequency is increased. Especially, arc pressure increases by 42.9 % at 40 kHz compared with that of C-GTAW process.

3.3. Weld bead geometry and heat input efficiency

The cross-sectional geometry of weld beads with average welding current at 80 A are shown in Fig. 9, which shows that weld penetration in the GTAW process is just 1.87 mm, while in the UHFP-GTAW process weld penetration varies from 2.13 mm to 2.4 mm when the pulse frequency increases from 20 kHz to 40 kHz. The depth-to-width ratio varying with different welding cases of C-GTAW, 20 kHz and 40 kHz follows a similar tendency to that of weld penetration. It can be concluded that UHFP-GTAW process has brought about a marked increase in weld penetration and depth-to-width ratio compared to GTAW process. It is supposed that larger arc pressure and more concentrated temperature distribution obtained by means of UHFP-GTAW process could result in digging effect on molten pool and improve the migration of molten pool liquid.

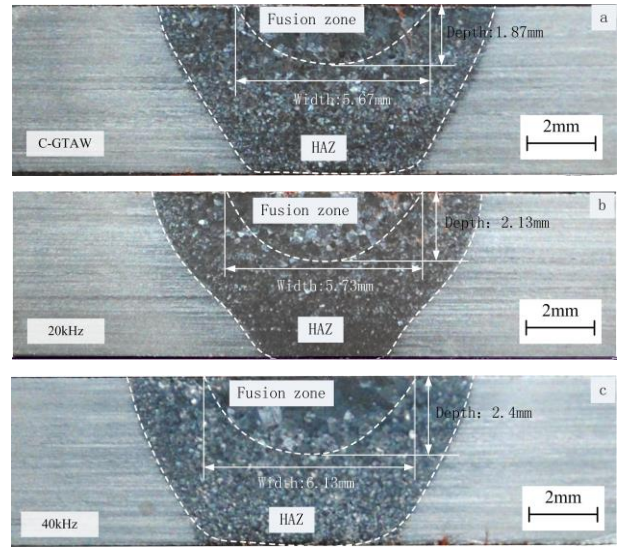


Fig. 9. Cross-sectional geometry of weld bead: a–C-GTAW; b– $f = 20 \text{ kHz}$; c– $f = 40 \text{ kHz}$

Corresponding to the latter three sets of process parameters listed in Table 3, the mean currents are all the same value of 80 A. It can be considered that the heat input of base metal obtained from welding arc is approximately equal under the three different process conditions. Thus the difference of weld shape can be attributed to the difference of heat input efficiency. The weld cross-sectional area is the direct reflection of heat input efficiency. In order to characterize heat input efficiency under different process conditions, image processing software named IMAGE-PRO PLUS was used to calculate the weld cross-sectional area under different process conditions. Corresponding to C-GTAW, 20 kHz and 40 kHz, the results calculated are 6.01 mm^2 , 7.89 mm^2 , and 9.68 mm^2 respectively. It can be concluded that heat input efficiency of UHFP-GTAW process is significantly higher than that of C-GTAW process, which led to cross-sectional area of the weld increased by at least 30 % under the given experimental conditions.

3.4. Weld bead microstructure

Grain structure in fusion zone was subsequently observed and analyzed. Concentrated heat input from the arc to the molten pool makes fusion zone undergo rapid melting and solidification process. Fig. 10 shows cross-sectional grain size and microstructure in fusion zone, which consists mainly of large-sized columnar crystal-based microstructure. Corresponding to C-GTAW, 20 kHz and 40 kHz, average intercept of grain in fusion zone is 0.305 mm, 0.240 mm and 0.210 mm respectively. In addition, grain size is reduced to 78.7 % and 68.9 % at 20 kHz and 40 kHz compared with that of C-GTAW process, which confirms that UHFP-GTAW process welded Ti-6Al-4V titanium alloy has the function of refining grain size and grain refinement becomes more significant with the increase of the pulse frequency.

Furthermore, microstructures were also observed by metallographic microscope with 100-times scale. Studies reported that, during welding process when the base metal is heated to temperatures over the β transus temperature, martensite phase transformation from the high-temperature

β phase would take place, and α would be formed with basket-weave [18]. In the UHFP-GTAW process, α martensite appears in the form of short acicular within the prior- β grains, and the distribution of basket-weave structure was also found to be expanded in fusion zone, which is particularly obvious with frequency of 40 kHz. By contrast, however, there was barely any basket-weave structure in fusion zone welded by C-GTAW process.

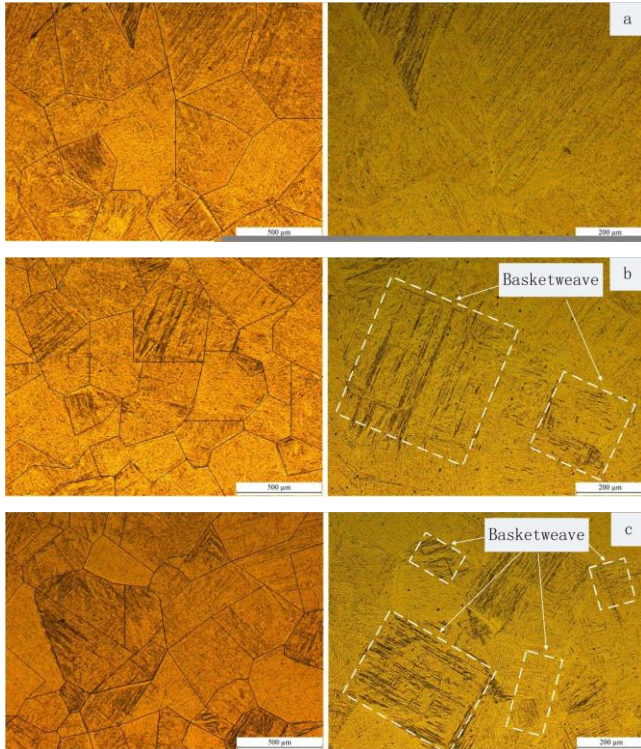


Fig. 10. Grain size and microstructure of fusion zone: a – C-GTAW process; b – $f = 20$ kHz; c – $f = 40$ kHz

3.5. Discussion

As shown in Fig. 11, arc pressure is primarily composed of electromagnetic pressure (p_e) and plasma jet pressure (p_p). The former is produced by the hybrid interaction effect between welding current and its self-induced electromagnetic field, while the latter is created by plasma motion due to the current density difference from tungsten tip (point A) to surface of workpiece (point B). It has been proved that pinch effect of arc column is initiated by electromagnetic force increment [19], and pulsed current with ultra-high frequency has the advantage of enhancing pinch effect. Radial component of electromagnetic force makes electric streamline close to the axis of the arc, while axial component of electromagnetic force will enlarge axial pressure exerting to molten pool.

During UHFP-GTAW process the core region of arc profile representing the high-temperature area of arc column would expand as average welding current increases. Besides, the higher the pulsed frequency, the larger the core region area. The reason for this is that higher pulse frequency make core region of arc column possess more concentrated heat input, and then more charged particles would be ionized, which increases the kinetic energy of arc plasma resulting in larger plasma jet force. With the

increase of axial electromagnetic force and axial plasma jet force, the degree of depression on the surface of molten pool will be aggravated, thus larger weld depth and higher depth-to-width ratio can be obtained.

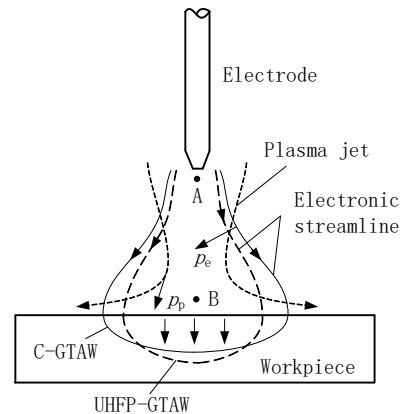


Fig. 11. Mechanism description of arc characteristics

Experimental results show that grain refinement occurred obviously in UHFP-GTAW process, and more basket-weave structure were also obtained, which helps to improve fracture toughness and fatigue properties of titanium alloy. It is analyzed that, during UHFP-GTAW process pulsed current makes the energy and the arc force exerting to the molten pool change periodically. the cyclic variations of energy would cause thermal fluctuations of molten pool which results in periodic interruption in the solidification process. Furthermore, the shape of molten pool takes on continual change, and hence the fluid motion and the convective of molten pool are also enhanced. The continual change in weld pool shape and the periodic interruptions in the growth process appear to inhibit the increase of crystallite size and lead to the refinement of the β grain structure. On the other hand, studies show that β grains tend to grow in the direction of the heat flow during the solidification process [18]. During UHFP-GTAW process arc force with strong stirring effect on the molten pool make the direction of heat flow irregular change, and thus the growth of each grain has not obvious orientation. As a result, each grain grows only a short distance, while more grains grow, which also leads to grain refinement to some extent. In addition, the enhanced fluid flow in UHFP-GTAW process decreases thermal gradient and reduces the cooling rate, which supposed to be the reason α martensite appears in the form of short acicular arranged in a crisscross pattern and wider distribution of basket-weave structure in fusion zone.

4. CONCLUSIONS

1. Compared with C-GTAW process, UHFP-GTAW process makes heat input more concentrated and leads to higher heat input efficiency, which can expand the core area of arc column with high temperature.
2. UHFP-GTAW process can produce larger arc pressure which can be increased by 42.9 % with pulse frequency at 40 kHz compared with that of C-GTAW process. Furthermore, the depth-to-width ratio enlarges with the increase of welding frequency.
3. Grain size is refined and reduced to 78.7 % ~ 68.9 %

in UHFP-GTAW process compared with that of C-GTAW process. Meanwhile, distribution of basket-weave structure expands in the fusion zone of Ti-6Al-4V titanium alloy welded by means of UHFP-GTAW process.

Acknowledgments

This research is supported by the National Natural Science Foundation of China under grant No. 51675052. We acknowledge and thus sincerely appreciate Beijing Institute of Petro-chemical Technology's substantial supports.

REFERENCES

1. **Jha, A.K., Singh, S.K., Kiranmayee, M.S., Sreekumar, K., Sinha, P.P.** Failure Analysis of Titanium Alloy (Ti6Al4V) Fastener Used in Aerospace Application *Engineering Failure Analysis* 17 (6) 2010: pp. 1457–1465. <https://doi.org/10.1016/j.engfailanal.2010.05.007>
2. **Cotton, J.D., Briggs, R.D., Boyer, R.R., Tamirisakandala, S., Russo, P., Shchetnikov, N., Fanning, J.C.** State of the Art in Beta Titanium Alloys for Airframe Applications *JOM* 67 (6) 2015: pp. 1281–1303. <https://doi.org/10.1007/s11837-015-1442-4>
3. **Ivasishin, O.M., Anokhin, V.M., Demidik, A.N., Savvakina, D.G.** Cost-Effective Blended Elemental Powder Metallurgy of Titanium Alloys for Transportation Application *Key Engineering Materials* 188 2000: pp. 55–62. <https://doi.org/10.4028/www.scientific.net/KEM.188.55>
4. **Zreiqat, H., Valenzuela, S.M., Nissan, B.B., Roest, R., Knabe, C., Radianski, R.J., Renz, H., Evans, P.J.** The Effect of Surface Chemistry Modification of Titanium Alloy on Signalling Pathways in Human Osteoblasts *Biomaterials* 26 (36) 2005: pp. 7579–7586. <https://doi.org/10.1016/j.biomaterials.2005.05.024>
5. **Köse, C., Karaca, E.** Effect of Pre and Post Weld Heat Treatments on the Microstructure and Mechanical Properties of Fiber Optic Beam Delivery System Assisted Robotic Nd:YAG Laser Welded Ti-6Al-4V Alloy *Archives of Metallurgy and Materials* 63 (3) 2018: pp. 1225–1233. <https://doi.org/10.24425/123795>
6. **Balasubramanian, M., Jayabalan, V., Balasubramanian, V.** Developing Mathematical Models to Predict Tensile Properties of Pulsed Current Gas Tungsten Arc Welded Ti-6Al-4V Alloy *Materials & Design* 29 (1) 2008: pp. 92–97. <https://doi.org/10.1016/j.matdes.2006.12.001>
7. **Balasubramanian, M., Jayabalan, V., Balasubramanian, V.** Effect of Pulsed Gas Tungsten Arc Welding on Corrosion Behavior of Ti-6Al-4V Titanium Alloy *Materials & Design* 29 2008: pp. 1359–1363. <https://doi.org/10.1016/j.matdes.2007.06.009>
8. **Sundaresan, S., Ram, G.D.J., Reddy, G.M.** Microstructural Refinement of Weld Fusion Zones in α - β Titanium Alloys using Pulsed Current Welding *Materials Science & Engineering A* 262 (1–2) 1999: pp. 88–100. [https://doi.org/10.1016/S0921-5093\(98\)01010-7](https://doi.org/10.1016/S0921-5093(98)01010-7)
9. **Balasubramanian, M., Jayabalan, V., Balasubramanian, V.** Effect of Pulsed Current Gas Tungsten Arc Welding Parameters on Microstructure of Titanium Alloy Welds *Journal of Manufacturing Science & Engineering* 131 (6) 2009: pp. 751–760. <https://doi.org/10.1115/1.4000373>
10. **Kumar, T.S., Balasubramanian, V., Sanavullah, M.Y.** Influences of Pulsed Current Tungsten Inert Gas Welding Parameters on the Tensile Properties of AA 6061 Aluminium Alloy *Materials & Design* 28 (7) 2007: pp. 2080–2092. <https://doi.org/10.1016/j.matdes.2006.05.027>
11. **Balasubramanian, M.** Prediction of Optimum Weld Pool Geometry of PCTIG Welded Titanium Alloy using Statistical Design *Engineering Science Technology, an International Journal* 19 (1) 2016: pp. 15–21. <https://doi.org/10.1016/j.jestech.2015.06.001>
12. **Ge, Z.X., Chen, H.M., Ge, Y.** Affection of Arc-weld Inversion Power's Frequency on Weld Grain's Thinning *Hot Working Technology* 7 2004: pp. 47–48. <https://doi.org/10.14158/j.cnki.1001-3814.2004.07.021>
13. **Balasubramanian, M., Ravisankar, V., Reddy, G.M.** Effect of Pulsed Current Welding on Mechanical Properties of High Strength Aluminum Alloy *International Journal of Advanced Manufacturing Technology* 36 (3) 2008: pp. 254–262. <https://doi.org/10.1007/s00170-006-0848-0>
14. **Babu, N.K., Raman, S.G.S.** Influence of Current Pulsing on Microstructure and Mechanical Properties of Ti-6Al-4V TIG Weldments *Science and Technology of Welding and Joining* 11 (4) 2006: pp. 442–447. <https://doi.org/10.1179/174329306X120750>
15. **Qi, B.J., Xu, H.Y., Zhou, X.G., Huang, S.T.** Fast Transform Ultra-sonic Pulse TIG Welding *Transactions of the China Welding Institution* 30 (7) 2009: pp. 57–60. <https://doi.org/10.3321/j.issn:0253-360X.2009.07.015>
16. **Qi, B.J., Yang, Z., Yang, M.X., Cong, B.Q.** Analysis on Characteristic of Ultra High Frequency Pulsed Gas Tungsten Arc Welding Process *Journal of Mechanical Engineering* 52 (2) 2016: pp. 26–32. <https://doi.org/10.3901/JME.2016.02.026>
17. **Qi, B.J., Yang, M.X., Cong, B.Q., Liu, F.J.** The Effect of Arc Behavior on Weld Geometry by High-frequency Pulse GTAW Process with 0Cr18Ni9Ti Stainless Steel *The International Journal of Advanced Manufacturing Technology* 66 (9–12) 2013: pp. 1545–1553. <https://doi.org/10.1007/s00170-012-4438-z>
18. **Köse, C., Karaca, E.** Robotic Nd:YAG Fiber Laser Welding of Ti-6Al-4V Alloy *Metals* 7 (6) 2017: pp. 221–231. <https://doi.org/10.3390/met7060221>
19. **Ando, K., Hasegawa, M.** Welding Arc Phenomenon, China Mechine Press, 1985: pp. 249–250.

